Calibration and Validation of the Dynamic Wake Meandering Model for Implementation in an Aeroelastic Code

H. Aa. Madsen
e-mail: hama@risoe.dtu.dk

G. C. Larsen

T. J. Larsen

N. Troldborg

Wind Energy Division,
Risø National Laboratory for Sustainable Energy,
Technical University of Denmark (DTU),
P.O. Box 49,
DK-4000 Roskilde, Denmark

R. Mikkelsen
Department of Mechanical Engineering,
MEK,
Fluid Mechanics Section,
Technical University of Denmark (DTU),
Nils Koppels Alle,
2800 Lyngby, Denmark

As the major part of new wind turbines are installed in clusters or wind farms, there is a strong need for reliable and accurate tools for predicting the increased loadings due to wake operation and the associated reduced power production. The dynamic wake meandering (DWM) model has been developed on this background, and the basic physical mechanisms in the wake—i.e., the velocity deficit, the meandering of the deficit, and the added turbulence—are modeled as simply as possible in order to make fast computations. In the present paper, the DWM model is presented in a version suitable for full integration in an aeroelastic model. Calibration and validation of the different parts of the model is carried out by comparisons with actuator disk and actuator line (ACL) computations as well as with inflow measurements on a full-scale 2 MW turbine. It is shown that the load generating part of the increased turbulence in the wake is due almost exclusively to meandering of the velocity deficit, which causes "apparent" turbulence when measuring the flow in a fixed point in the wake. Added turbulence, originating mainly from breakdown of tip vortices and from the shear of the velocity deficit, has only a minor contribution to the total turbulence and with a small length scale in the range of 10–25% of the ambient turbulence length scale. Comparisons of the calibrated DWM model with ACL results for different downstream positions and ambient turbulence levels show good correlation for both wake deficits and turbulence levels. Finally, added turbulence characteristics are compared with correlation results from literature.
[DOI: 10.1115/1.4002555]

1 Introduction

The most common methodology for the prediction of fatigue loads in wake operation is the approach where the influence of the wake is taken into account by introducing an increased, effective turbulence in the aeroelastic simulations. This increased turbulence depends on a number of parameters such as distance to the upstream turbine, turbine loading, component Wöhler exponent, and ambient turbulence. A description of this methodology and the research behind it can be found in the comprehensive report by Frandsen [1]. It is also at present the recommended method to take into account wake operation in The International Electrotechnical Commission (IEC) standard [2] for wind turbines.

However, often the aeroelastic analysis of wind turbines operating in wakes requires a more detailed modeling of the wake conditions. One example concerns the details of yaw loads, which were one of the reasons to start the development of the DWM model presented first by Madsen et al. [3]. Later the model was applied also to the extreme response prediction in Thomsen and Madsen [4]. Another example where a detailed modeling of the physical flow mechanisms in the wake structure is needed is for advanced control developments based on individual pitch control or on flap control. It is important to be able to model correctly the influence of the ambient turbulence levels and in particular the very low turbulence levels observed on offshore sites. Finally, an integrated modeling of both the increased loading and the reduced power production is desirable for wind farm optimization.

Although computational fluid dynamics (CFD) modeling of wakes has been presented several years ago by, e.g., Sørensen and Shen [5] and Alinot and Masson [6], it seems that it is first within the past few years that CFD wake simulations really have advanced our insight in the wake flow mechanisms for real turbines in the atmospheric boundary layer flow. In particular, the modeling of turbulent atmospheric inflow in combination with the actuator line (ACL) model for wake flow simulations as presented by Troldborg et al. [7] seemed to model the basic wake flow mechanisms. The results presented in this paper show the strong influence ambient turbulence has on the break down of the tip vortices as well as on the meandering of the wake. The influence of ambient turbulence on tip vortex breakdown was also studied in detail by Ivanell [8] using the ACL model.

A detailed analysis of wind farm production and the increased loading can thus be extracted from CFD modeling of wakes based on actuator disk (AD) models or ACL models using turbulent inflow conditions corresponding to atmospheric flow. However, the simulation time is still so high that design and optimization analysis of wind farms is a challenging task using these advanced models.

There is thus a need for reliable engineering wake prediction models. The DWM model was developed on this background, and the objective was to model the basic wake flow mechanisms with sufficient accuracy while keeping the model as simple as possible. The underlying hypothesis in the DWM model is that the wake deficit from the upstream turbine, in combination with meandering of this deficit, is the major contributor to the increased loading. The detailed formulation of the meandering mechanism applied in the DWM model has been described by Larsen et al. [9]. However, the meandering of the wake and its influence on the fatigue and extreme loading on a downstream turbine seems not to have been given much attention in the past and was only briefly considered in the review study on wakes by Vermeer et al. [10]. However, Ainslie [11,12] discussed the subject in more detail and

Contributed by the Solar Energy Division of ASME for publication in the JOURNAL OF SOLAR ENERGY ENGINEERING. Manuscript received July 13, 2009; final manuscript received September 2, 2010; published online October 14, 2010. Assoc. Editor: Spyros Voutsinas.

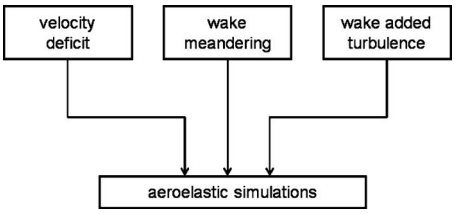

Fig. 1 The main elements of the DWM model

modeled the effect from wake meandering on mean wake deficits by correlating the wake meandering to the variability in the wind direction.

Since the first formulation of the DWM model in 2003 [3,4], there has been a development in the different parts of the model. Added wake turbulence was considered in Ref. [13], and a major development of the model, including the computation of the initial velocity deficit behind the rotor, made it possible to include the DWM model fully in an aeroelastic code, which is presented in Ref. [14]. The present paper presents the model in this latter version as it is implemented in the aeroelastic code HAWC2. The focus is on a detailed calibration of model parameters and on model validation. Three different sources are used for calibration and validation: (1) actuator disc (AD) simulations, (2) ACL simulations, and (3) inflow measurements on a full-scale turbine operating in wake conditions (experimental data).

The paper is organized in the following way. First, the DWM model is described. Then follows a short description of the two numerical models and the experiment used for deriving the calibration and validation results. Results on the computation of the initial deficit and its downstream development are then presented, followed by a section showing the influence of ambient turbulence. Added wake turbulence is then considered, and finally, a paragraph with the results of the final calibrated model is presented by showing velocity deficits and turbulence intensity distributions in the wake at different downstream positions and for different ambient turbulence levels. In addition, the spectra of the different turbulence components are shown.

2 DWM Model

The DWM model comprises three essential corner stones—namely, a model for the computation of the quasi-steady velocity deficit and its development downstream, a model of the downstream wake meandering process, and finally, a model of the added wake turbulence. The model is schematically illustrated in Fig. 1.

The *quasi-steady velocity deficit* is formulated in the moving (meandering) frame of reference, and it includes the wake expansion as a function of downstream transportation time caused by turbulence diffusion and, initially, also by the rotor pressure field. The *wake meandering model* describes the stochastic downstream transport of the upstream emitted wakes driven by large scale turbulence structures, which are assumed not to be significantly affected by the presence of a wind turbine. The *turbulence effects* within the meandering wake, caused by an upstream located turbine, concern small-scale turbulence with characteristic eddy sizes up to approximately one rotor diameter and include contributions from conventional mechanically generated turbulence caused by the wake shear as well as from the shed vorticity from the blades consisting mainly of tip and root vortices.

The involved submodels are treated separately in the succeeding subsections along with a description of the integration of these models in the framework of the aeroelastic code HAWC2.

2.1 Quasi-Steady Velocity Deficit. The first version of the DWM model complex [3,4] was based on quasi-steady velocity deficits computed in a loop, involving a coupling between an external CFD actuator disk model of the rotor-wake interaction and an aeroelastic model. However, in order to obtain a fully *integrated* formulation of the deficit prediction in the framework of an aeroelastic code, the quasi-steady wake deficit prediction has been reformulated. The present formulation is based on the assumption that the velocity deficit can be computed on the basis of the inductions in the rotor plane and in the far wake using the blade element momentum (BEM) theory in combination with the boundary layer approximation of the Navier–Stokes equations to model the downstream development of the deficit. The derivation has the following three steps:

1. Initially, the "start" deficit is determined by calculating the induced velocities in the rotor plane for the wake generating turbine in question.
2. Subsequently, the expansion of the computed rotor plane deficit in the near wake region is determined. This expansion is primary driven by the pressure recovery in the near wake regime.
3. Finally, the development (i.e., expansion and attenuation) of the velocity deficit, as function of the downstream distance from the wake generating turbine, is quantified, taking into account the turbulent mixing caused by both ambient turbulence and by the turbulence generated by the wake shear field itself. This model is based on a thin shear layer (TL) approximation of the Navier–Stokes equations in their rotational symmetric form.

2.1.1 Step 1. In a first approximation, we assume *uniform inflow* conditions on the wake generating turbine—i.e., the effect of possible inflow wind shear profiles on the wake generation is excluded. This restriction is mainly introduced to match the description of the wake expansion described in item "Step 3," where rotationally symmetric wake deficits are also assumed.

Based on the uniform inflow, induced velocities in annular rotor plane elements are calculated based on BEM theory. Blade pitch angles and rotor rotational speed are chosen to match the "*mean operational condition*" of the turbine in question at the selected wind speed.

2.1.2 Step 2. The "initial" expansion of the wake, caused by the pressure rise in the *near wake region*, is calculated based on mass and momentum balance considerations. Denoting the uniform rotor inflow wind speed by U_0 and the axial interference factor by a, the wake velocity along a stream line is reduced to $U_2=U_0(1-2a)$ at downstream distances where the pressure loss has recovered, whereas the velocities at the rotor plane are reduced to $U_1=U_0(1-a)$. In the present context, we interpret the *near wake regime* as the regime extending from the rotor plane to the downstream distance where the pressure loss has recovered (i.e., typically the region within two to three rotor diameters downstream).

To match the BEM approach, we assume that the above relations hold not only along a particular stream line but also within annular stream tubes bounded by stream lines. Within this extension influence factors, characteristic for particular stream lines are replaced with influence factors characteristic for particular stream tubes. Discretizing the radial coordinate in agreement with the BEM discretization (see Fig. 2), the mass flow, $\dot{m}_i$, through the ith annular stream tube, extending from $r_{t,i}$ to $r_{t,i+1}$ at the rotor plane and from $r_{w,i}$ to $r_{w,i+1}$ at the downstream border of the near wake regime may be expressed as

$$\dot{m}_i = \pi\rho U_0(1-a_i)(r_{t,i+1}^2 - r_{t,i}^2), \quad i=1,\ldots,N-1 \tag{1}$$

and

$$\dot{m}_i = \pi\rho U_0(1-2a_i)(r_{w,i+1}^2 - r_{w,i}^2), \quad i=1,\ldots,N-1 \tag{2}$$

respectively, where N denotes the number of radial stations defined in the rotor plane. Assuming incompressibility, the continuity equation simply dictates the mass flows, expressed in Eqs. (1) and (2), to be equal. This leads to an expression of the radius of

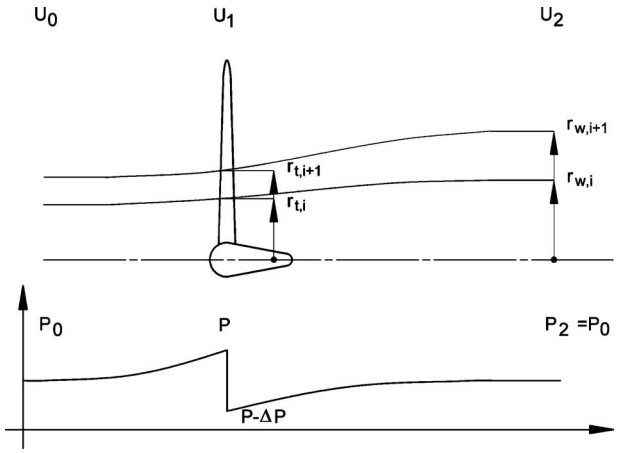

Fig. 2 Wake expansion of an annular BEM stream tube due to pressure changes in the near wake region

the $(i+1)$th far wake radius in terms of the *local* stream tube induction a_i, the ith far wake radius, and the ith and $(i+1)$th rotor radii. Consequently, we have the following simple iterative scheme for the determination of the discretized radial coordinate in the wake at the downstream border of the near wake regime:

$$r_{w,i+1} = \sqrt{\frac{1-a_i}{1-2a_i}(r_{t,i+1}^2 - r_{t,i}^2) + r_{w,i}^2}, \quad i = 1, \ldots, N-1 \tag{3}$$

The initial value $r_{w,1}$ is 0.0.

A discrete representation of the wake deficit U_w, as a function of radial coordinate at the downstream border of the near wake region, is thus finally defined as

$$U_w((r_{w,i+1} + r_{w,i})/2) = U_0(1-2a_i), \quad i = 1, \ldots, N-1 \tag{4}$$

where the average stream tube radius has been taken as the characteristic radial coordinate for the stream tube. With this approach, an additional radial coordinate is required to complete the downstream wake deficit description at the wake outer radius where the flow velocity for continuity reasons has to take the value of the ambient flow,

$$U_w(r_{w,N}) = U_0 \tag{5}$$

The discretized wake representation defined by relations (4) and (5) is subsequently used as input to the modeling of the wake expansion further downstream as described in "step 3." Note that flow velocities taking a uniform value, equal to the ambient flow velocity U_0, outside the wake outer radius is a simplification since mass conservation implies higher flow velocities in the flow regime outside the wake. However, proper accounting of this feature requires (at least) a two-dimensional modeling setup with, e.g., a radial coordinate included in the flow equations.

2.1.3 Step 3. The development of the velocity deficit in the far wake regime (i.e., the downwind wake region extending beyond the near wake region) is mainly affected by turbulent mixing. The present formulation of the model, handling the expansion of the wake deficit caused by turbulent mixing, is strongly inspired by the work of Ainslie [11,12,15].

We describe the turbulent mixing, occurring outside the near wake region, in terms of the rotationally symmetric Navier–Stokes equations with the pressure terms disregarded. Moreover, the gradients of mean flow quantities are assumed much bigger in the radial direction (denoted by r) than in the axial direction (denoted by x), which leads to the *thin shear layer (TL) approximation* of the rotationally symmetric Navier–Stokes equations. The momentum equation part of these equations may be expressed as

$$U\frac{\partial U}{\partial x} + V_r\frac{\partial U}{\partial r} = -\left(\frac{1}{r}\right)\frac{\partial}{\partial r}(r\overline{uv_r}) \tag{6}$$

where U and V_r denote the mean velocity in the axial and radial directions, respectively, u and v_r denote the respective fluctuating velocity components in these directions, and an upper bar denotes temporal averaging.

Introducing the eddy viscosity concept, the Reynolds stresses are expressed as

$$-\overline{uv_r} = \nu_T\frac{\partial U}{\partial r} \tag{7}$$

with the eddy viscosity given by

$$\nu_T = l_m U_{mi} \tag{8}$$

where U_{mi} and l_m are suitable velocity and length scales of the turbulence that in general will vary with the downstream distance x but assumed *independent* of the radial coordinate r. The length and velocity scales are taken to be proportional to the *instantaneous* wake half width b, and the maximum deficit velocity difference, $(U_0 - U_{\mathrm{def,min}})$, across the wake shear layer, respectively, where U_0 and $U_{\mathrm{def,min}}$ denote the ambient wind speed and the minimum wake wind speed, respectively. Introducing Eqs. (7) and (8) into Eq. (6), the governing momentum equation is reformulated as

$$U\frac{\partial U}{\partial x} + V_r\frac{\partial U}{\partial r} = \left(\frac{\nu_T}{r}\right)\frac{\partial}{\partial r}\left(r\frac{\partial U}{\partial r}\right) \tag{9}$$

with

$$\nu_T = F_2 k_2 b(U_0 - U_{\mathrm{def,min}}) + F_1\nu_{TA} \tag{10}$$

where k_2 is an empirical *constant* for the wake flow field and F_1 and F_2 are filter functions depending on only the downstream position x. The calibration of constant k_2 and of filter functions will be detailed in Sec. 4. The second term in Eq. (10), ν_{TA}, is the viscosity term depending on the ambient turbulence level. Following the approach of Ainslie [11], ν_{TA} is linked to the atmospheric boundary layer parameters where the turbine is operating. The following correlation of ν_{TA} to the surface roughness length z_0 is proposed by Ainslie [11]:

$$\frac{\nu_{TA}}{U_H D} = \frac{\kappa^2}{\ln\left(\frac{z_H}{z_0}\right)} \tag{11}$$

where U_H is the wind speed at hub height, κ is the von Karman constant, z_H is the turbine hub height, D is the rotor diameter, and z_0 is surface roughness length.

We now make the following derivations in order to link ν_{TA} directly to the ambient turbulence intensity I_{amb}. For neutral atmospheric conditions, the Monin–Obukhov scaling dictates the standard deviation of the velocity fluctuations δ to be proportional to the friction velocity u_* and therefore invariant through the boundary layer [16].

Thus,

$$\sigma = \alpha u_* \tag{12}$$

with α being the proportionality constant. With convection neglected, the logarithmic law for the vertical mean wind field further applies whereby

$$\bar{V}(z) = \frac{u_*}{\kappa}\ln(z/z_0) \tag{13}$$

where z is the measuring altitude.

Combining equations Eqs. (12) and (13) leads to the following simple relation between the site turbulence intensity I_{amb} and the altitude z

$$I_{\text{amb}}(z) = \frac{\alpha\kappa}{\ln(z/z_0)} \tag{14}$$

where the parameter $\alpha \approx 2.4$ according to Ref. [16].

Combining Eq. (10), (11), and (14), we obtain

$$\frac{\upsilon_T}{U_H R} = F_2 k_2 \left(\frac{b}{R}\right)\left(1 - \frac{U_{\text{def,min}}}{U_H}\right) + F_1 2\frac{I_{\text{amb}}\kappa}{\alpha} \tag{15}$$

where we have nondimensionalized with the rotor radius R and I_{amb} is now the turbulence intensity at hub height. It should be noted that as we have assumed an axisymmetric flow model, we set U_0 equal to U_H. Finally, denoting the nondimensional eddy viscosity υ_T^* and introducing a calibration constant k_{amb}, which contains both the values of α and κ (i.e., 2.4 and 0.4) and a calibration taking into account that not all the scales of the ambient turbulence will influence the downstream development of the deficit, we get the following expression for υ_T^*:

$$\upsilon_T^* = F_2 k_2 \left(\frac{b}{R}\right)\left(1 - \frac{U_{\text{def,min}}}{U_H}\right) + F_1 k_{\text{amb}} I_{\text{amb}} \tag{16}$$

The calibration of F_1 and k_{amb} will be shown later in the paper.

In addition to the momentum Eq. (9), the flow must fulfill the continuity equation given by

$$\frac{1}{r}\frac{\partial}{\partial r}(rV_r) + \frac{\partial U}{\partial x} = 0 \tag{17}$$

The flow problem defined by Eqs. (9) and (17) is solved numerically using a finite difference scheme, with initial conditions defined by the downstream wake deficit obtained from the "step 2" approach.

2.2 Conventional Turbulence Characteristics. The total turbulence intensity in wake affected flows I_{tot} is composed of three turbulence sources: ambient turbulence intensity I_{amb}, apparent turbulence intensity from meandering I_m, and finally, added wake turbulence intensity I_{aw}. According to the terminology, as for example used by Vermeer et al. [10], the added turbulence intensity due to the presence of the turbine is then derived from the total wake turbulence intensity and ambient turbulence intensity by the relation

$$I_{\text{add}} = \sqrt{I_{\text{tot}}^2 - I_{\text{amb}}^2} \tag{18}$$

However, as will become clear in Sec. 2.5, the turbulence in the DWM model is the result of linearly adding the different turbulence velocity components.

2.3 Wake Turbulence in the Meandering Frame of Reference. Added wake turbulence includes contributions from conventional mechanically generated turbulence, caused by the *wake shear*, as well as from the shed *blade bound vorticity*, consisting mainly of the tip and root trailing vortices. The vortices will initially take the form of organized coherent flow structures but later, due to instability, will gradually break down and approach the characteristics of conventional turbulence—although with modified turbulence characteristics compared with atmospheric turbulence. In analogy with the description of the wake deficit, we aim at a description of the added wake turbulence in the meandering frame of reference.

The wake turbulence, at a particular downstream position, is modeled based on a *homogeneous* Mann turbulence field [17] with cross sections of the turbulence box covering one rotor diameter. The resolution of the turbulence box is high (i.e., 128 $\times$ 128 points) in planes perpendicular to the mean flow direction to allow small turbulence eddies to be resolved reasonably well. The length of the turbulence box in the mean flow direction is 4800 m with a resolution of 1024 points. The added turbulence refers to the meandering frame of reference, and the center position of the turbulence box thus follows the center position of the associated wake deficits. Although violating the second order statistics of the turbulence field, the *inhomogeneity* of the added turbulence is approximated by a simple scaling of the created homogeneous Mann field. *Rotationally symmetry* of added wake turbulence intensity is assumed, resulting in a scaling coefficient depending on the radial rotor coordinate only. The selected scaling factor k_{mt} depends on the quasi-steady *deficit depth* at the considered downstream distance as well as on the *deficit gradient* according to

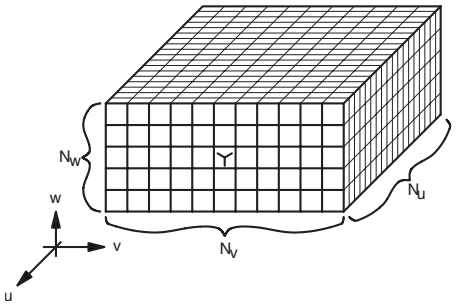

Fig. 3 Layout of the turbulence box used for generating the meander turbulence. A coarse grid resolution (size of 1 rotor diameter) is used in the in-plane (v, w) directions, whereas the resolution in the u-direction is chosen to be fine. The symbol "Y" indicates the rotor position.

$$k_{mt}(r) = |1 - U_{\text{def}}(r)|k_{m1} + \left|\frac{\partial U_{\text{def}}(r)}{\partial r}\right| k_{m2} \tag{19}$$

where $U_{\text{def}}(r)$ is nondimensionalized with U_H and r with R. Two empirical factors k_{m1} and k_{m2} are introduced to schedule the gain of these two contributions.

Determination of the specific characteristics of I_{aw} will be discussed later as well as the calibration of the constants k_{m1} and k_{m2}.

2.4 Wake Meandering. The wake meandering part is based on a *fundamental presumption* stating that the transport of wakes in the atmospheric boundary layer can be modeled by considering the wakes to act as *passive tracers* driven by the *large-scale* turbulence structures. Modeling of the meandering process consequently includes considerations of a suitable description of the "carrier" stochastic transport media as well as of a suitable definition of the cutoff frequency defining large-scale turbulence structures in this context. The modeling and simulation of the meandering path have been described in Ref. [9], and validation based on full-scale measurements of the instantaneous wake position obtained from LiDAR recordings has been presented [18,19]. Only the specific implementation of the meandering process in HAWC2 is described here.

The turbulence field chosen as the stochastic transport media generating the wake meandering is the Mann turbulence model [17] since this turbulence field offers correlation between the u, v, and w turbulence components formulated in Cartesian coordinates and further enables unequal grid resolution and size in the three directions (see Fig. 3).

A coarse grid resolution is chosen in the in-plane directions since this, first of all, enables an effective cutoff frequency filtering, neglecting all eddies with a size less than the rotor, and second, it enables very large spatial dimensions of the box, which is especially important if several wake sources are considered. A special feature when using several upstream wake sources in the same turbulence field is that if a wake passes the center of the next turbine, the two wakes will remain together for the rest of the transport since they meet the same turbulence. The grid resolution in the u-direction is chosen with a finer resolution in order to get a smooth continuous variation in deficit center positions. It is important that the grid point velocities represent the mean value of a grid cube in order to provide a correct spatial filtering.

2.5 Adding Turbulence Velocity Components. To summarize, the total turbulence in the wake contains contributions from meandering (apparent turbulence) from added wake turbulence and from ambient turbulence. The velocity components are interrelated

$$U = U_m + u_{\text{aw}} + u_{\text{amb}} \tag{20}$$

where U denotes the axial velocity in the resulting flow field, u_{aw} and u_{amb} are the axial velocity components from added wake turbulence and ambient turbulence, respectively. U_m is the unsteady velocity component from meandering of the velocity deficit determined as

$$U_m = U(x_m, r_m) \tag{21}$$

where r_m is the local coordinate in a reference system (axisymetric deficit) following the meandering wake center and coupled to the global reference system by the position of the downstream turbine (x_t, y_t, z_t) and the meandering position (y_m, z_m) of the wake updated at each time step.

The lateral and vertical turbulent velocity components v, w are derived in the same way except that they do not contain a component from meandering,

$$v = v_{\text{aw}} + v_{\text{amb}} \tag{22}$$

where v_{aw} is the lateral velocity component of added wake turbulence and v_{amb} is the lateral velocity component of ambient turbulence.

Likewise,

$$w = w_{\text{aw}} + w_{\text{amb}} \tag{23}$$

where w_{aw} is the lateral velocity component of added wake turbulence and w_{amb} is the lateral velocity component of ambient turbulence.

3 Numerical Models and Experiment for Calibration and Validation

We used three sources to obtain the data material for calibration and validation of the DWM model, and these are described briefly below.

3.1 Actuator Disk Model Computations. The general purpose CFD code FIDAP [20] is used for the AD computations, which will be used for calibration and validation of the quasi-steady velocity deficit and its downstream development. In the past, this code has been used for several studies using the actuator disk theory. The previous studies comprised, among others, comparisons with the BEM model, influence of turbulent mixing and high loading [21], and yawed flow aerodynamics [22,23]. Based on experiences from these studies, the setup used for the present simulations was as follows: axisymmetric flow, a mesh stretching $10R$ in the upstream and radial directions and $40R$ in the downstream direction, a disk covered by two layers of elements in the streamwise direction, and a total extension of 0.05. Finally, a k-ε turbulence model was used with a Reynolds number of 10^4 based on the rotor radius.

3.2 Actuator Line Computations

.

3.2.1 Actuator Line Model. The actuator line model was developed by Sørensen and Shen [5]. The model combines the three-dimensional Navier–Stokes solver ELLIPSYS3D, developed by Michelsen [24,25] and Sørensen [26], with a technique in which body forces are distributed radially along lines representing the blades of the wind turbine. Thus, the flow field around and downstream the wind turbine is governed by full three-dimensional Navier–Stokes simulations using large eddy simulation (LES), whereas the influence of the rotating blades on the flow field is computed by calculating the local angle of attack of the flow to determine the local forces from tabulated airfoil data.

3.2.2 Atmospheric Boundary Layer Model. The atmospheric boundary layer is modeled using a technique where body forces applied to the entire computational domain is used to impose a given but arbitrary steady wind shear profile while free-stream turbulence was modeled by introducing synthetic turbulent velocity fluctuations to the mean flow upstream the rotor.

The method of prescribing a given wind shear profile by imposing body forces was presented by Mikkelsen et al. [27] and is essentially based on the immersed boundary technique.

The atmospheric inflow turbulence was simulated using a technique [7] where unsteady concentrated body forces, introduced in a plane located one rotor radius upstream the wake generating rotor, are producing the synthetic turbulent velocity fluctuations. The introduced turbulence field was generated in advance by using the Mann algorithm [17], which simulates homogenous, stationary, Gaussian, and anisotropic turbulence with the same spectral characteristics as observed in the atmosphere.

3.2.3 Computational Domain and Boundary Conditions. The computations were conducted in a Cartesian computational mesh with dimensions $28R$ in the flow direction, $24R$ in the vertical direction, and $24R$ in the lateral direction. A high concentration of grid points was distributed equidistantly in the region around and downstream of the rotor in order to preserve the generated flow structures in the wake. In the equidistant domain, a rotor radii was resolved with 30 grid points and outside this region grid points were stretched away toward the outer boundaries. The grid consisted of 144 grid points in the cross-flow directions and 768 grid points in the flow direction.

The boundary conditions were as follows. The velocity was specified according to the wanted shear profile at the inlet, unsteady convective conditions at the outlet, no-slip at the ground, far-field velocity at the top boundary and periodic conditions on the sides.

3.3 Full Scale Experiment on 2 MW Turbine. Inflow measurements with a five-hole pitot tube on the blade of a 2 MW NM80 turbine are used in the present paper for validation of intensity of added turbulence. The instrumented turbine is situated in the Danish Tjaereborg wind farm sited on a flat and inhomogeneous terrain close to the sea. In the direction southwest to the instrumented turbine, four NM80 turbines are aligned in a row, and a number of different wake situations can thus be measured for the instrumented turbine. The present analysis focuses on wake situations caused by the closest of these turbines, which is positioned about 3.3 rotor diameters upstream in a direction of 205 deg. Inflow measurements and structural measurements have been reported in more detail for this turbine [13], but in the present paper only the spectra of the relative velocity measured by the five-hole pitot tube will be used. The NM80 turbine will also be used for the simulations with the ACL and DWM model.

4 Calibration and Validation of Quasi-Steady Wake Deficit Computation

Calibration of the quasi-steady wake deficit was first done on the basis of results from a uniformly loaded actuator disk. In order to check separately the start deficit, which is the input to the TL model and derived from Eqs. (3) and (4), we wanted to correlate the AD and TL velocity profiles as close as possible to the rotor disk but on the other hand avoid a major contribution from the pressure field around the disk, which is not modeled in the TL model. A distance of $2D$ downstream was chosen, and the axial velocity profiles for the two models are compared in Fig. 4, left part. However, as seen on the AD results, the turbulent mixing has already at this point influenced the velocity profile, as it is not completely rectangular. Therefore, the TL computations are run from the rotor disk and downstream, and for the first distance of $2D$ a suitable low eddy viscosity was chosen (adjusted by the filter function F_2), which gave the same slope of the TL velocity profile

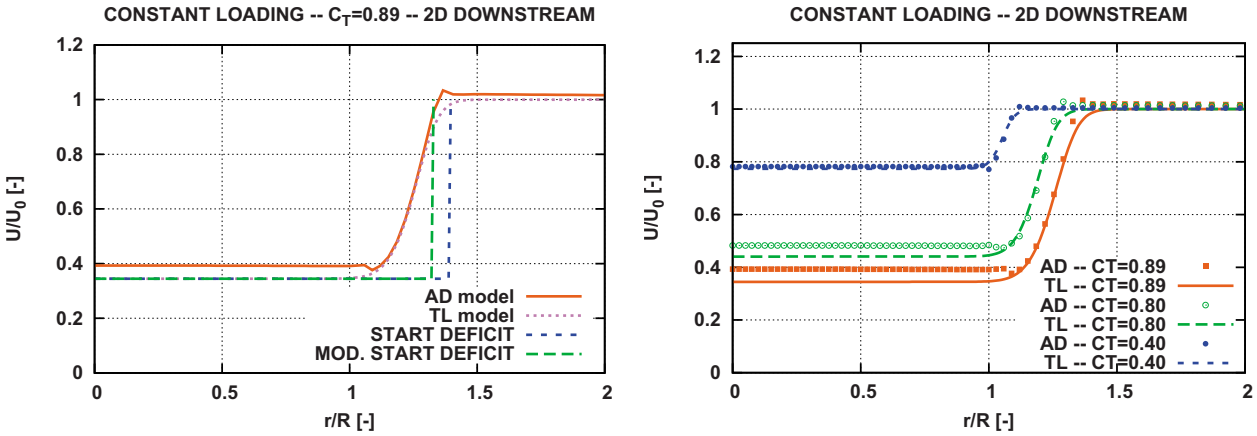

Fig. 4 Left: the initial deficit and the modified initial deficit used as input for the TL model compared with the AD model 2*D* downstream. Right: comparison of TL and AD model for different loadings.

when compared with the AD profile. However, it turned out from the comparisons that the expansion predicted by Eqs. (3) and (4) was slightly too high, and the following correction was applied:

$$f_w = 1 - 0.45a_{\text{av}}^2 \tag{24}$$

where a_{av} is the average induction factor over the rotor disk. The factor f_w is afterward multiplied on the radial positions given by Eq. (3),

$$r_{w,i} = r_{w,i} f_w \tag{25}$$

Using this correction on the expansion, a good correlation between TL and AD profiles was found for different loadings, as seen in the right part of Fig. 4. The difference in the depth of the deficits is mainly due to the influence from the pressure field, which is not modeled in the TL approach and which in the AD results, at a distance of 2*D* downstream, has not disappeared completely.

Next, the eddy viscosity in Eq. (10) was calibrated in the *far wake* to give the same slope of the TL deficit data as the AD results. The constant k_2 was in this way calibrated to 0.008, assuming the filter function F_2 to take the value 1 here. Finally, the correlation of the TL and AD results in the range from 2*D* to 10*D*, Fig. 5, determined the filter function F_2 shown in Fig. 6. The reason to introduce the filter function was discussed by Ainslie [15] and is the lack of equilibrium between the velocity field and the developing turbulence in the early stages of the wake flow. Having calibrated the TL model as relating to uniform loading, it was next tested by computations on the NM80 turbine at 6 m/s (Fig. 7). To the left is shown the development of the velocity deficits at different radial stations, and in general, the correlation with the AD results is good. In particular, the transition to the bell formed deficit at around 10*D* downstream is well predicted. Also, the correlation between the axial and radial velocity profiles at a downstream position of 6*D*, shown to the right in Fig. 7, is good.

5 Calibration and Validation of the Influence of Ambient Turbulence

The calibration of the influence of ambient turbulence, which concerns the filter function F_1 and the parameter k_{amb} in Eq. (16), was carried out on the basis of ACL simulations on the NM80 turbine run at different ambient turbulence levels: 0%, 5%, 10%, and 15%. A technique [19] was implemented to detect the position of the instantaneous deficit at a specific downstream position for each time step, and, finally, all these deficits were assembled to obtain an average deficit in the meandering frame of reference. On the basis of this data set, axial velocities at two radial positions, r/R=0.8 and r/R=0.0, were extracted and shown as functions of the downstream position for the four different ambient turbulence levels in Fig. 8 (right) and Fig. 9 (right).

Before calibrating k_{amb} in the DWM model, the filter function F_1 was defined. The motivation for introducing this function is mainly that the TL model simulations are run from the position of the wake generating turbine and downstream and with the starting deficit as defined above. However, in the real world, the actuator disk pressure field gives a continuous decrease in the velocities

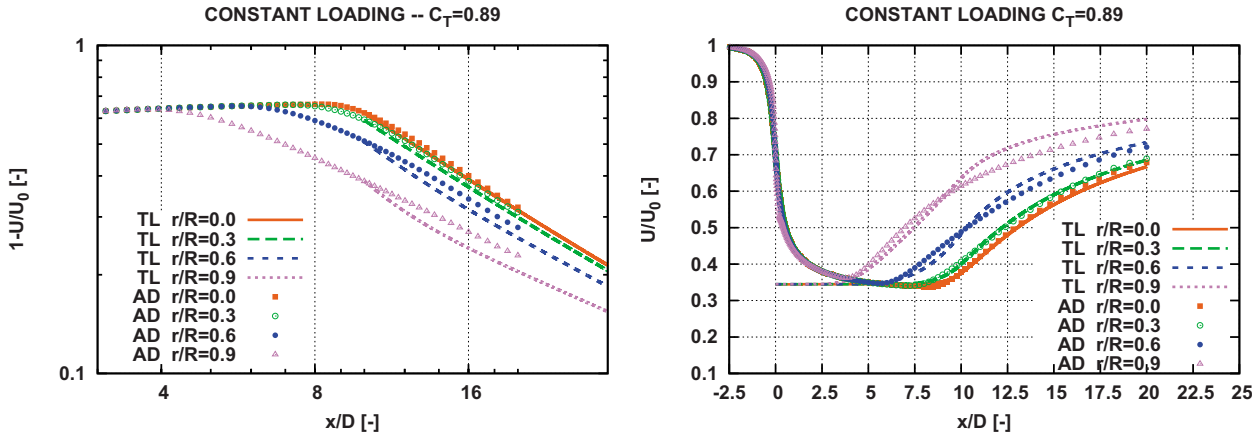

Fig. 5 Comparison of AD computations with calibrated TL model predictions

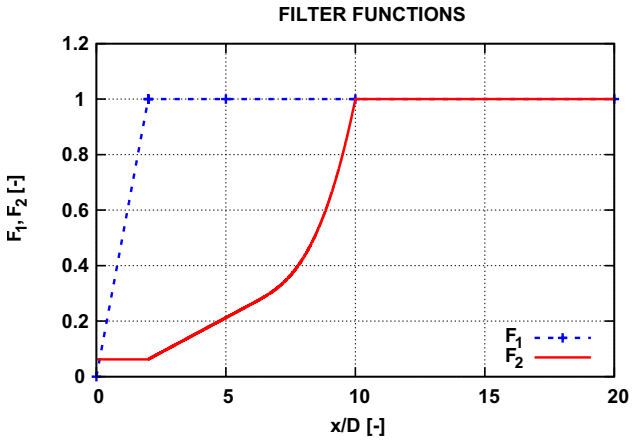

Fig. 6 The filter function F_2 derived on basis of results in Fig. 5 and F_1 derived on basis of the results in Figs. 8 and 9

down to a position of $2-3D$ behind the rotor disk. Therefore, we have chosen the F_1 filter function to vary linearly from 0 to 1 over the distance 0 to $2D$ (Fig. 6). Subsequently, the DWM model was run with different values of k_{amb} at the same ambient turbulence levels as the ACL simulations, and a value of 0.07 was found to give the best correlation (cf. Fig. 8 (left) and Fig. 9 (left)). The correlation is, in general, best for $r/R=0.8$, whereas a bigger impact of the ambient turbulence is seen on the DWM model along the center line than that predicted with the ACL model.

The importance of the k_{amb} parameter for the intensity I_m of the turbulence generated by meandering is illustrated by the graphs in Fig. 10 (left), showing I_m at two downstream positions computed with values of k_{amb} equal to 0.07 and 0.0, respectively. The value of 0.0 reflects that the ambient turbulence has no influence on the development of the quasi-steady deficit. It is seen that turbulence increases considerably when the k_{amb} factor is reduced to zero, which is simply because the meandering velocity deficit is more pronounced in this situation. To the right in Fig. 10 is shown how the turbulence develops downstream for the same two values of k_{amb}. It should finally be noted that the simulations presented in Fig. 10 were run with I_{aw} equal to zero, so that the turbulence shown is only due to meandering of the deficit.

6 Calibration and Validation of the Influence of Added Turbulence

The first investigation on implementing added wake turbulence (I_{aw}) in the DWM model was presented in Ref. [13] on the basis of full-scale measurements of inflow and blade root moments on the NM80 2 MW turbine in the Tjaereborg wind farm. The main problem of extracting I_{aw} from experiments is to separate this type of turbulence from ambient turbulence and in particular from the turbulence contribution I_m originating from meandering of the ve-

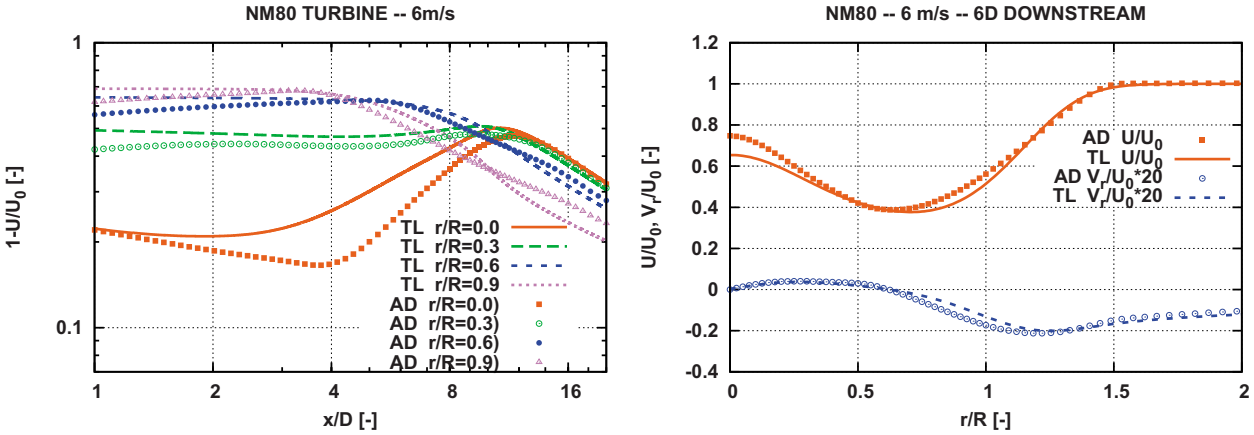

Fig. 7 Computations on the NM80 turbine with the calibrated TL model and compared with AD results. Left: downstream development of the velocity deficit at different radial positions; right: distribution of axial and radial velocity $6D$ downstream.

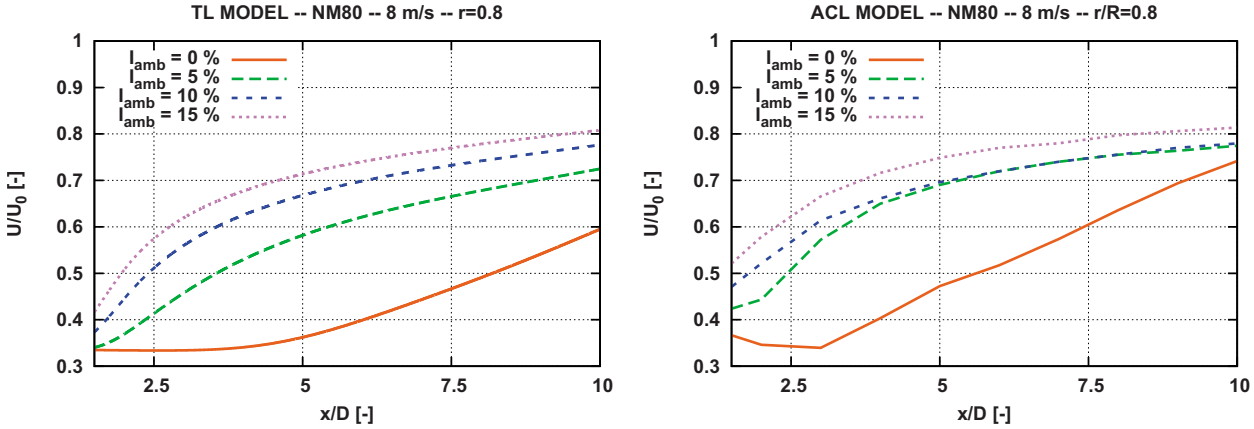

Fig. 8 Final calibrated influence of ambient turbulence on development of axial velocity deficit downstream by comparing the TL results (to the left) with ACL simulations (to the right) with simulations representing different ambient turbulence levels. Computations on the NM80 turbine at 8 m/s at radius 0.8.

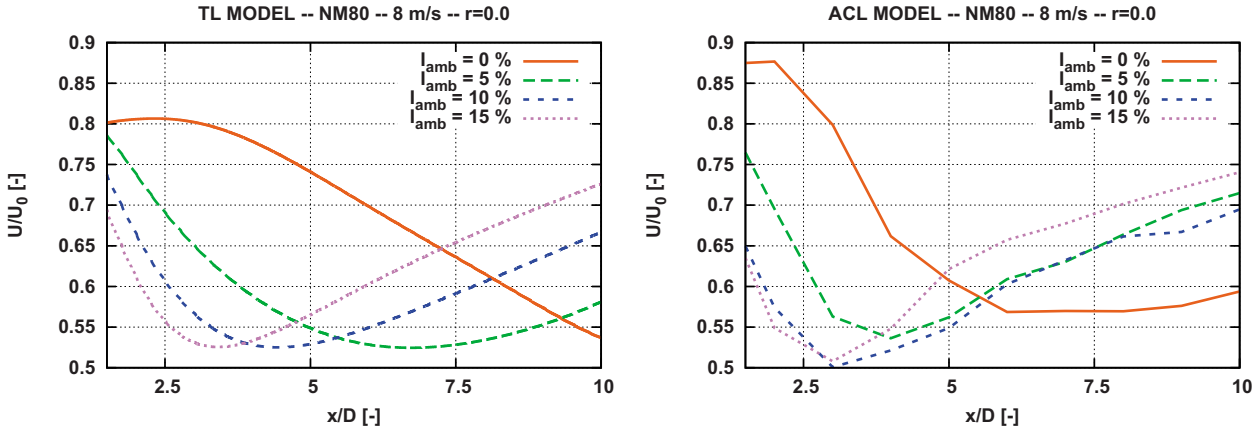

Fig. 9 Final calibrated influence of ambient turbulence on development of the axial velocity deficit downstream by comparing the TL results (to the left) with ACL simulations (to the right) with simulations representing different ambient turbulence levels. Computations on the NM80 turbine at 8 m/s at radius 0.0.

locity deficit. However, using measurements recorded at very low ambient turbulence (2–3%), the influence from meandering is modest, and in this way it was possible to identify and quantify the added turbulence in both the inflow data and the structural data from the Tjaereborg turbine [13]. In particular, the standard deviation of the relative velocity on the blade is a good measure for added turbulence, as meandering only slightly influences this velocity component. Concerning the structural measurements, the influence of added turbulence could be seen as a high number of small fatigue cycles when compared with the DWM model without added turbulence, which indicated that added turbulence has a length scale significantly smaller than that of the ambient turbulence. A length scale of 8 m (referring to the Mann turbulence model) was estimated. Later, the first real implementation of added turbulence in the DWM model was presented in Ref. [14] based on ACL computations and the NM80 measurements. The present implementation of added turbulence is the same as presented in Ref. [14], however, with a few changes of the parameters as discussed below on basis of a more detailed analysis of the ACL computations [28].

The ACL computations simulated the NM80 turbine at a low wind speed situation (5 m/s) and thus a high thrust coefficient of 0.87 for a fast break up of the tip vortices. The analysis of the wake flow was performed 7*D* downstream and was based on a 26.5 min long time series. Assuming rotational symmetry, an azimuthal averaging of the data for a given radial position could be performed. The power spectra (PSD) for the axial and transversal turbulence velocity components, u and v, as shown in Fig. 11, are typically composed of an energy-containing subrange characterized by low frequency components of limited statistical significance, an inertial subrange with a spectral gradient close to $-2/3$ in agreement with the theoretical expectation, and a dissipation subrange which, in the case of these numerically based spectra, results from the limited spatial resolution as well as from numerical diffusion. Further confidence in the added wake turbulence extracted from the ACL simulations is gained from the results presented in Fig. 12 where the frequency averaged ratios between u spectral values and the corresponding v and w spectral values are presented as functions of the normalized wake radius. For an incompressible fluid, the second Kolmogorov similarity assumption dictates this ratio to be 3/4 assuming *local* homogeneity [29], which is in excellent agreement with the reported results. The degree of *isotropy* of added wake turbulence is enlightened by computing the *turbulent energy*, expressed in terms of root mean square, and the *turbulence length scales* for the three turbulence components at the investigated radial positions. For defining the length scale, we use here the (one-sided) Kaimal spectrum as the generic spectrum to which the observed spectra will be fitted, thus following the procedure outlined in Ref. [28]. The results are summarized in Table 1.

As seen, the degree of isotropy, quantified in terms of root

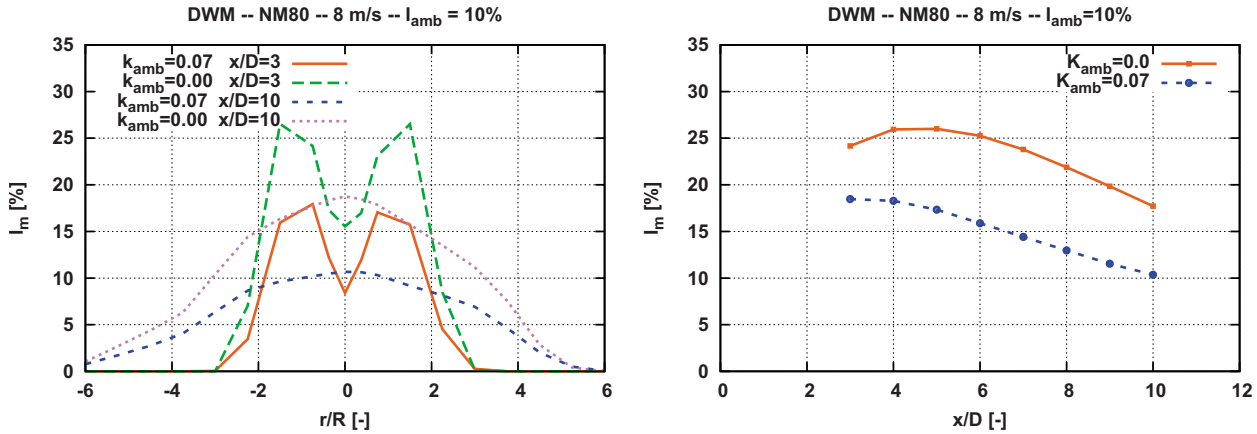

Fig. 10 Left: distribution of the turbulence generated by meandering of the deficits computed with the DWM model at two different downstream positions and for two different values of the parameter k_{amb}. Right: downstream development of turbulence from meandering at a radius of 0.75 for two different values of k_{amb}.

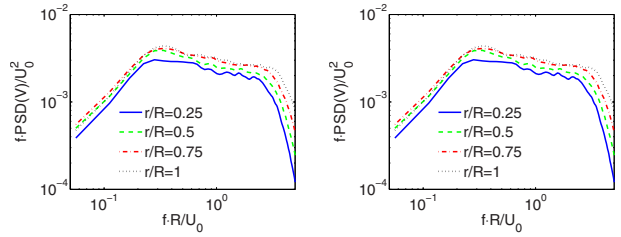

Fig. 11 Left: spectra of the *u*-turbulence component at different radial positions 14*R* downstream simulated with the ACL model in conditions corresponding to no ambient turbulence. Right: the same for the v turbulence component.

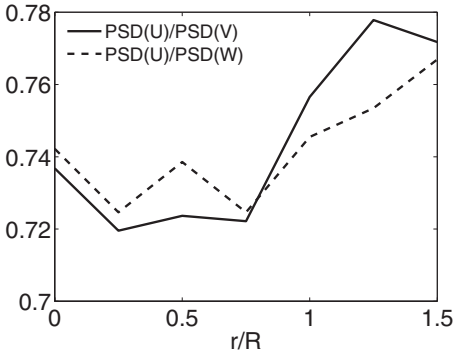

Fig. 12 Ratio of PSD spectra of the *u*, *v*, and *w* turbulence components computed with the ACL model 14*R* downstream

Table 1 Top part of table: root mean square of turbulence components at different radial stations. Lower part of table: turbulence length scales (corresponding to Kaimal turbulence parametrization) of various turbulence components at different radial positions.

	σ_u/U_0 [m^2/s^2]	σ_v/U_0 [m^2/s^2]	σ_w/U_0 [m^2/s^2]
0.25*R*	0.108	0.112	0.117
0.50*R*	0.120	0.123	0.125
0.75*R*	0.130	0.130	0.133
1.00*R*	0.139	0.133	0.138
	L_u/R	L_v/R	L_w/R
0.25*R*	1.16	0.27	0.33
0.50*R*	1.06	0.27	0.30
0.75*R*	0.93	0.26	0.27
1.00*R*	0.65	0.24	0.24

mean square of the added wake turbulence, is close to perfect for the investigated radial positions. For the quantification in terms of length scale, however, isotropic characteristics are only obtained for the lateral and vertical turbulence components. For ideal isotropic turbulence, the turbulence length scales associated with the lateral and vertical turbulence components should be identical [17], which is clearly demonstrated for the computed turbulence. The turbulence scale associated with the longitudinal turbulence component, however, should be of the order 1.45 times the other two length scales [17]. This is not reflected in the computed added wake turbulence where this factor varies in the range 4.29 to 2.70. However, the 1.45 ratio extracted from Ref. [17] is based on an assumption of homogeneous turbulence and the added wake turbulence is clearly inhomogeneous.

For use in the DWM simulations, we chose, based on the above results, a length scale for the u turbulence component equal to 1.0*R* (i.e., approximately 40 m with reference to a Kaimal spectral parametrization). However, for generating the added turbulence, we use the Mann turbulence and the above Kaimal length scale of 40 m corresponds to a length scale of approximately 3.8 m in the Mann formalism.

Using a Mann turbulence box for added isotropic turbulence with a length scale of 3.8 m, the parameters k_{m1} and k_{m2} in the DWM model (see Eq. (19)) were determined by correlating with ACL results for the NM80 turbine at 5 m/s and no ambient turbulence, see Fig. 13. The ACL results at three different downstream positions show clearly that it takes some time before the added turbulence reaches its maximum value, most probably corresponding to the time required for the tip vortices to completely break down. The time constant relating to the breakdown of the tip vortices has not yet been modeled in the DWM model where the strength only depends on the shape of the quasi-steady deficit. One of the reasons not to include this is that it might be equally important to model that the breakdown of the tip vortices is accelerated by the level of ambient turbulence, as predicted by Ivanell [8]. So, in general, there will be ambient turbulence and it is expected that the tip vortex breakdown will take place within the first 3–5*D* downstream.

The calibrated added turbulence was subsequently tested on inflow measurements on the NM80 turbine at low wind speed (5–6 m/s) and thus also a high thrust coefficient and at very low ambient turbulence intensity in the range 2–3% [13]. A study of the correlation between inflow measurements on the rotor and the turbulence in a fixed frame of reference was presented recently by Madsen and Fischer [30].

Within about 1 h, the wind direction changed slowly, so that measurements within this short time interval could be performed in free inflow, about 1/3 wake loading (part of azimuth with wake

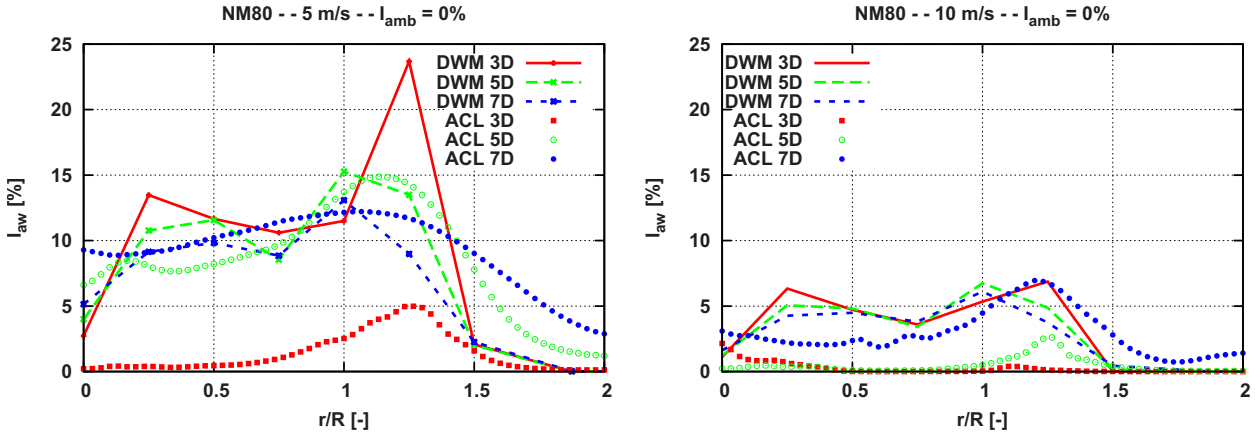

Fig. 13 Comparison of added turbulence predicted by the ACL and DWM model after calibration of the two parameters k_{m1} and k_{m2} in Eq. (19). The ACL simulations were conducted without ambient turbulence. Left: results at different downstream positions for a 5 m/s inflow situation. Right: the same for a 10 m/s inflow situation.

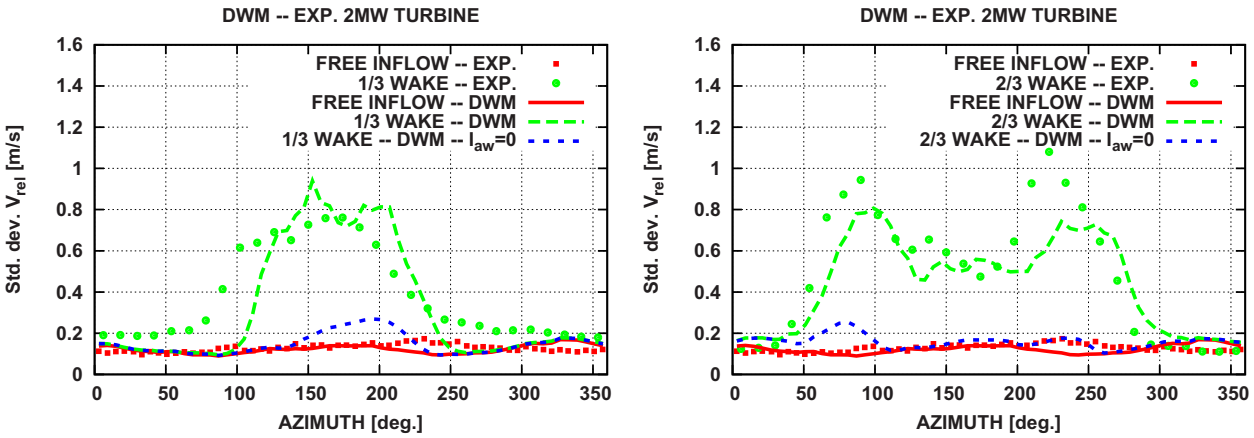

Fig. 14 Simulations on the NM80 turbine in three inflow conditions at low ambient turbulence (2–3%) with the DWM model with calibrated added turbulence as shown in Fig. 13. Wind speed around 5–6 m/s. Standard deviation of the relative velocity at radius 24 m on the blade is shown. To the left, free inflow and 1/3 wake operation at 3.5*D* downstream and to the right, free inflow and 2/3 wake operation at 3.5*D* downstream.

flow) and 2/3 wake loading, see Fig. 14. The standard deviation of the relative velocity V_{rel}, measured with the five-hole pitot tube at radius 24 m, is shown in comparison with standard deviation of V_{rel} from the DWM model. Both the single peak shape, corresponding to the 1/3 wake loading and the double peak shape, corresponding to the 2/3 wake loading, is captured well in the DWM model as well as the level of standard deviation. To illustrate that the standard deviation on V_{rel} mainly is due to the added turbulence, the model results without added turbulence are also shown.

7 Results From Final Calibrated DWM Model and Discussion

In this section, we show results from the final calibrated DWM model in comparison with ACL results for the NM80 turbine at 8 m/s and at downstream stream distances of 3*D*, 6*D*, and 10*D* and for ambient turbulence levels of 5%, 10%, and 15%. Further, the downstream development of the added wake turbulence in comparison with results from Jimenez et al. [31] is shown.

To summarize the following calibrated parameters were used in DWM model: $k_{m2}=0.008$, $k_{amb}=0.07$, $k_{m1}=0.6$, and $k_{m2}=0.35$ and the filter functions F_1 and F_2 shown in Fig. 6. Finally, for the added turbulence, we used isotropic Mann turbulence with a length scale of 5 m, which is about 14% of the length scale used for the ambient turbulence and for the large scale meandering turbulence box.

Before comparing with the ACL model, results only from the DWM model are presented in order to show the relative contribution from meandering and from added turbulence to the total turbulence level in the wake (see Fig. 15). The model was run with and without added turbulence, and as seen on the turbulence levels across the wake (see Fig. 15, left), added turbulence contributes only with a very small part to the total turbulence. To the right in Fig. 15, the spectra of the axial flow component inside the wake at a radial position equal to the rotor radius in comparison with the spectrum of the ambient wind speed are shown. It is seen that the spectra qualitatively are similar but with a tendency that the spectral slope in the inertial subrange of the wake turbulence being slightly smaller. It also appears that the added turbulence is only seen in the spectrum for frequencies above 0.4–0.6 Hz.

Next, the comparison of the DWM and ACL results for the NM80 turbine at 8 m/s are shown in Figs. 16 and 17. In general, a good correlation for the velocity deficits is found at the closest downstream distances and for the lowest ambient turbulence levels (see Fig. 16). The wake center peak in velocity is only found for a distance of 3*D* and a turbulence of 5% in both models. The rise in center velocity as function of downstream distance is al-

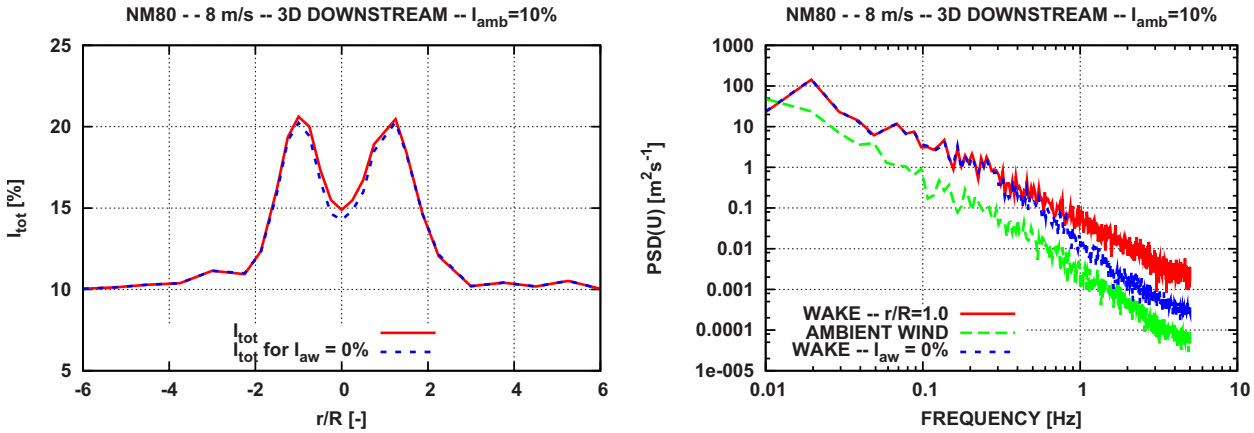

Fig. 15 Left: total turbulence intensity 3*D* downstream predicted with the DWM model for the NM80 at 8 m/s and I_{amb} =10%. Model runs with and without added turbulence. Right: power density spectra of the axial turbulence component of the ambient wind, the wake at radius *r*=*R* and the wake simulated without added turbulence.

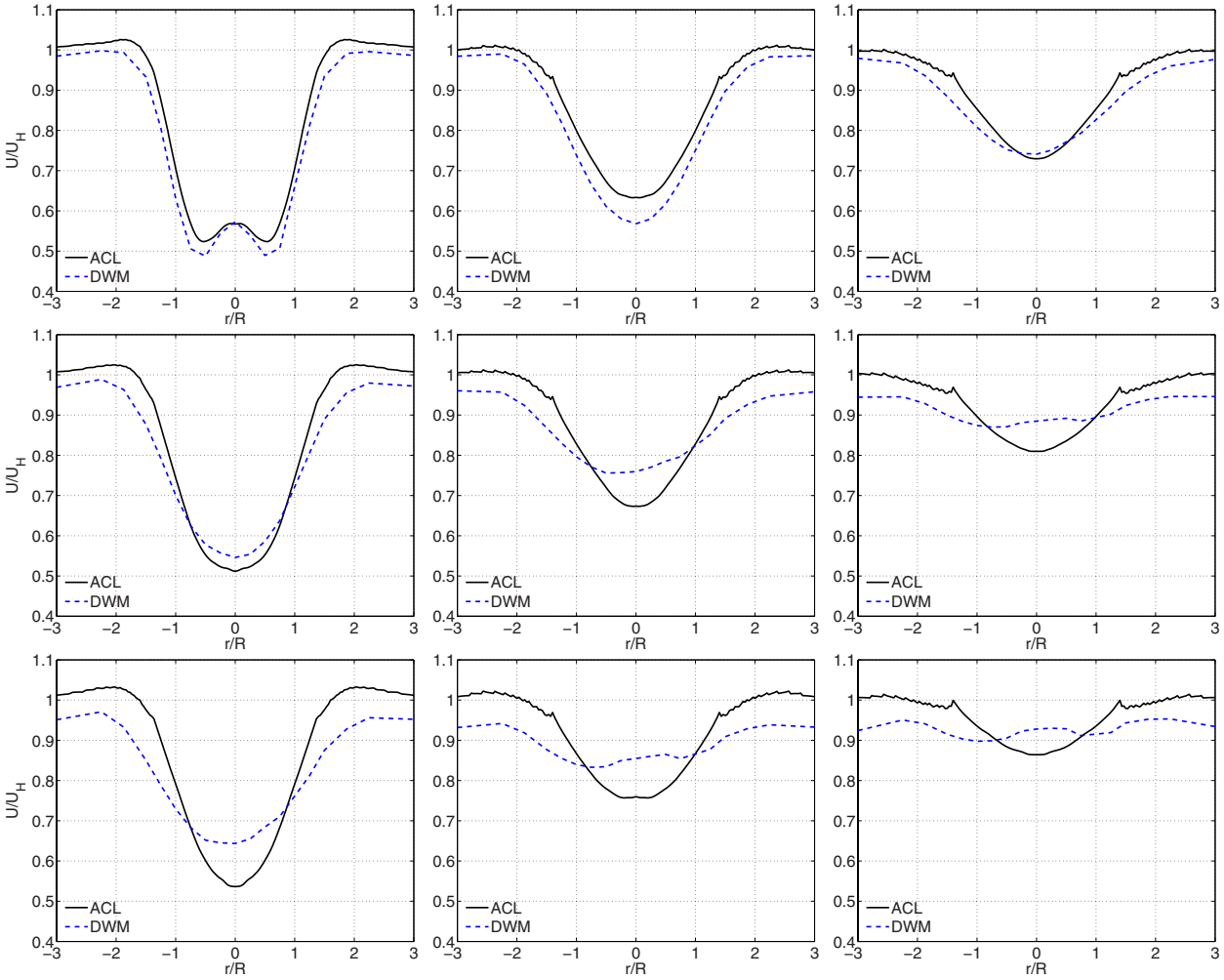

Fig. 16 Comparison of the DWM model with ACL results for the NM80 turbine at 8 m/s, downstream positions of 3*D*, 6*D*, and 10*D* (from left to right in the figure) and for 5%, 10%, and 15% ambient turbulence (from top to bottom). The nondimensional axial velocities are shown.

most perfect for 5% ambient turbulence. Concerning the increasing deviations for increasing turbulence and distance, they seem to be due to a smaller meandering in the ACL model. This is most probably due to the limited width of the turbulence box (320 m or four rotor diameters) used in the ACL model simulations, which as a consequence restricts the size of the largest scales of the ambient turbulence. However, also for 10% and 15% ambient turbulence, the rate of increase in center velocity is predicted well by the DWM model, although the absolute velocities are slightly higher.

In analogy with the tendencies for the velocity deficits, the correlation between ACL and DWM predicted levels of total turbulence, as shown in Fig. 17, is also best for the lowest ambient turbulence levels. The match at 3*D* distance and 5% turbulence is almost complete with two distinct peaks in the turbulence intensity.

These peaks disappear gradually for increasing downstream distance as well as for increasing turbulence intensity. It seems that the DWM model predicts turbulence that is somewhat above the ACL model results, in particular for high turbulence levels and for the biggest downstream distances. This indicates a somewhat lower meandering, which is in agreement with the tendency in the velocity deficits. The question is then if there is too low meandering in the ACL model or too high meandering in the DWM model. A comparison with experimental data is one of the possibilities for further investigations on this.

Finally, a comparison is shown in Fig. 18 of the added wake turbulence computed with the DWM model for the NM80 turbine at three different wind speeds, 6 m/s, 8 m/s, and 10 m/s and at two different levels of ambient turbulence, 5% and 10%, respectively, with the LES results of Jimenez et al. [31] including the correlation curves of Frandsen and Thögersen [32], of Quarton and Ainslie [33], and of Crespo and Hernández [34]. One important characteristic of the DWM results is the strong dependence on the ambient turbulence where it is seen that the added turbulence increases considerably with decreasing ambient turbulence. The same qualitative relation is modeled by Crespo and Hernandez [34] in their correlation function for added turbulence, whereas Quarton and Ainslie [33] models a decrease in added turbulence for a decrease in ambient turbulence. Another characteristic of the DWM results is that the influence of wind speed and thus also of the thrust coefficient is mainly seen for distances below 10 rotor diameters.

8 Conclusions

The DWM model has been presented in a version suitable for fully integration in an aeroelastic code. In the present case, the DWM model has been implemented in the HAWC2 code, which takes about 2% more computation time when used together with the DWM model. Although an axisymmetric model is used for the computation of the initial velocity deficit and its subsequent de-

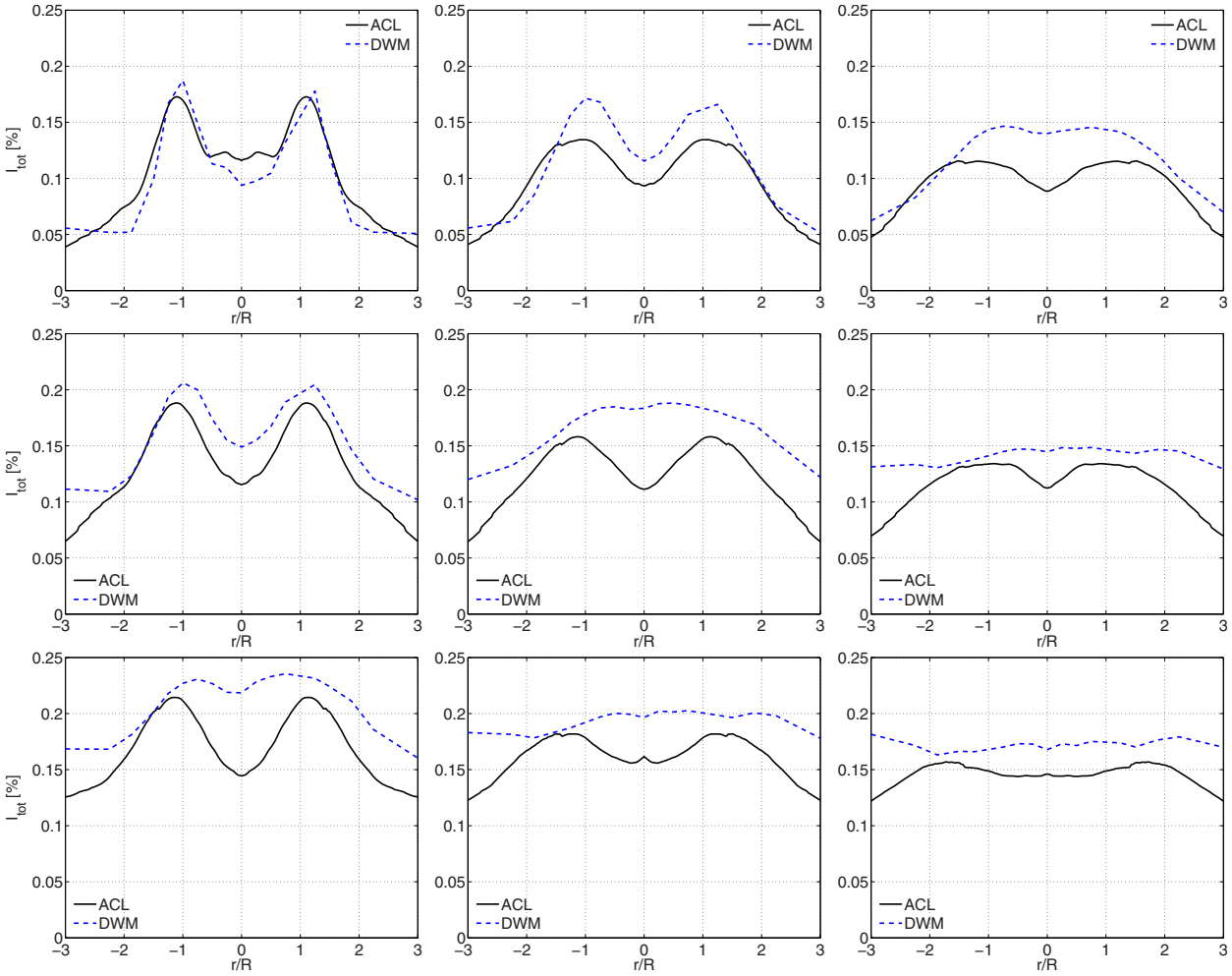

Fig. 17 Comparison of the DWM model with ACL results for the NM80 turbine at 8 m/s, downstream positions of 3*D*, 6*D*, and 10*D* (from left to right in the figure) and for 5%, 10%, and 15% ambient turbulence (from top to bottom). The total turbulence intensity is shown.

velopment downstream under influence of turbulent mixing, the deficit is imposed on the ambient flow field with turbulence and shear. The resulting turbulence characteristics from meandering of the wake will thus generally not be axisymmetric.

The computation of the quasi-steady deficit and its development has been calibrated using AD simulations in flow cases in the absence of ambient turbulence. The influence of ambient turbulence and added turbulence was calibrated using ACL simulations. Using the final calibrated DWM model, the wake deficit and the wake turbulence have been compared with the ACL model for different ambient turbulence levels and downstream positions. The influence of these two important parameters seems, in general, to be well predicted.

The results also show that almost all of the wake generated turbulence is due to the meandering of the quasi-steady velocity deficit causing "apparent turbulence" when measuring at a fixed point in the wake. By apparent, it means that the origin of the turbulence is quite different from the normal turbulence—namely, by stochastic meandering of an organized flow structure. The spectrum of the wake flow is comparable in shape to the spectrum of ambient velocity. Finally, the total added turbulence due to wake operation is shown to increase considerably for decreasing ambient turbulence, which is qualitatively in agreement with the correlation function for the added turbulence proposed by Crespo and Hernandez [34] but opposite to that by Quarton and Ainslie [33].

Acknowledgment

The work has been funded by the European Commission in the framework of the Non-Nuclear Energy Programme Sixth Framework under Contract No. REN07/FP6EN/S07.73680/038641 (TOPFARM—Next Generation Design Tool for Optimization of Wind Farm Topology and Operation).

Nomenclature

a = axial induction in the BEM code
a_{av} = average induction
b = wake half width (m)
D = rotor diameter (m)
f = frequency (rad/s)
f_w = calibration factor on wake deficit expansion
F_1 = filter function for ambient velocity
F_2 = filter function for self-generated turbulence
i = stream tube number
I_{amb} = ambient turbulence intensity
I_{add} = total added turbulence intensity in the wake
I_m = turbulence intensity from meandering
I_{aw} = turbulence intensity from added wake turbulence
I_{tot} = total turbulence intensity in the wake
k_2 = calibration factor for self-generated turbulence

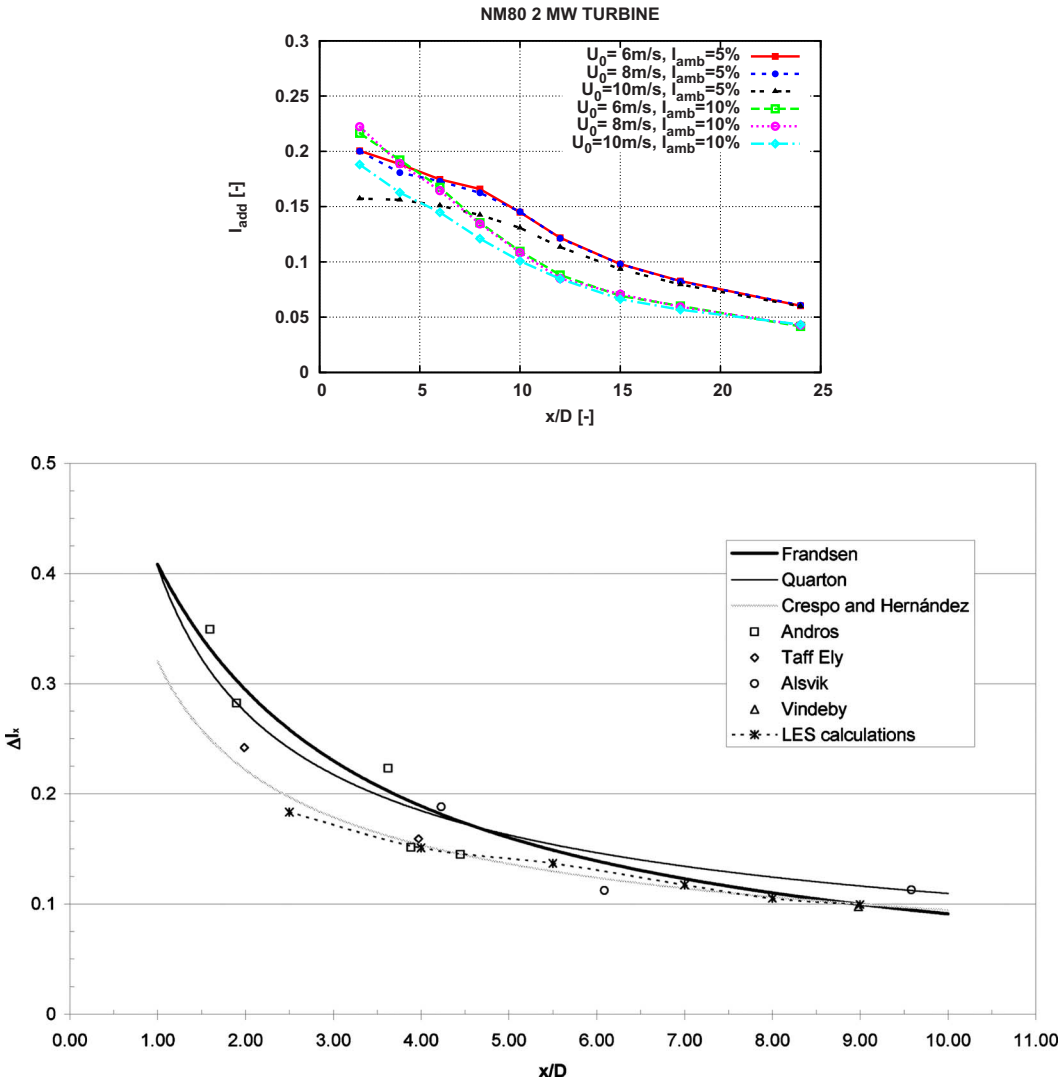

Fig. 18 The upper figure shows the added turbulence computed with the DWM model for the NM80 turbine at three different wind speeds and two different ambient turbulence levels. The lower figure is from Jiminez et al. [31] and shows added turbulence computed with a LES model in comparison with empirical correlation curves from literature as well as experimental results.

k_{amb} = calibration factor for influence of ambient turbulence
k_{m1} = calibration factor for added turbulence, influence of velocity deficit
k_{m2} = calibration factor for added turbulence, influence of velocity gradient
l_m = mixing length (m)
N = number of radial positions on rotor plane
r = radial position (m)
r_m = local radial coordinate in the meandering coordinate system (m)
R = rotor radius (m)
u = turbulent velocity component in mean flow direction (m/s)
u_{amb} = turbulent velocity component from ambient wake turbulence (m/s)
u_{aw} = turbulent velocity component from added wake turbulence (m/s)
u^* = friction velocity (m/s)
U = axial flow velocity component (m/s)
U_0 = ambient wind speed or free wind speed (m/s)
U_1 = wind speed at rotor disk (m/s)
U_2 = far wake wind speed (m/s)
U_{def} = wake deficit velocity (m/s)
$U_{def,min}$ = minimum wake deficit velocity across the wake (m/s)
U_m = unsteady velocity component from meandering of velocity deficit (m/s)
U_{mi} = characteristic velocity for derivation of the eddy viscosity (m/s)
U_w = initial wake wind speed (m/s)
v = turbulent velocity component in lateral direction (m/s)
v_{amb} = lateral turbulent velocity component from ambient turbulence (m/s)
v_{aw} = lateral turbulent velocity component from added wake turbulence (m/s)
V = lateral flow velocity component (m/s)
w = vertical turbulent velocity component (m/s)
w_{amb} = vertical turbulent velocity component from ambient turbulence (m/s)
w_{aw} = vertical turbulent velocity component from added wake turbulence (m/s)
W = vertical flow velocity component (m/s)

V = radial flow velocity component (m/s)
x = distance downwind from turbine, flow direction (m)
y = lateral position (m)
y_m = lateral position of the center of the meandering velocity deficit (m)
z = altitude (m)
z_0 = surface roughness length
z_H = hub height (m)
z_m = vertical position of the center of the meandering velocity deficit (m)
α = empirical constant
σ = standard deviation of velocity fluctuations (m/s)
σ_u = standard deviation of axial flow velocity component (m/s)
σ_v = standard deviation of transversal velocity component (m/s)
σ_w = standard deviation of vertical velocity component (m/s)
κ = von Karman constant
ν_T = eddy viscosity (m^2/s)
ν_{Ta} = eddy viscosity from ambient turbulence (m^2/s)
$\bar{\cdot}$ = temporal averaging

References

[1] Frandsen, S., 2003, "Turbulence and Turbulence Generated Structural Loading in Wind Turbine Clusters," Risø Report No. Risø-R-1188(EN).
[2] 2004, "Wind Turbines. Part 1: Design Requirements," Report No. IEC 61400-1.
[3] Madsen, H. A., Thomsen, K., and Larsen, G. C., 2003, "A New Method for Prediction of Detailed Wake Loads," Proceedings of the IEA Joint Action of Wind Turbines 16th Symposium, S.-E. Thor, ed., pp. 171–188.
[4] Thomsen, K., and Madsen, H. A., 2005, "A New Simulation Method for Turbine in Wakes—Applied to Extreme Response during Operation," Wind Energy, **8**, pp. 35–47.
[5] Sørensen, J. N., and Shen, W. Z., 1999, "Computation of Wind Turbine Wakes Using Combined Navier Stokes/Actuator-Line Methodology," Proceedings of the European Wind Energy Conference EWEC '99, Nice, Italy.
[6] Alinot, C., and Masson, C., 2002, "Aerodynamic Simulations of Wind Turbines Operating in Atmospheric Boundary Layer With Various Thermal Stratifications," ASME Wind Energy Symposium, 40th Collection of Technical Papers, Reno, Paper No. AIAA-2002-42.
[7] Troldborg, N., Sørensen, J. N., and Mikkelsen, R., 2007, "Actuator Line Simulation of Wake of Wind Turbine Operating in Turbulent Inflow," J. Phys.: Conf. Ser., **75**, pp. 012063.
[8] Ivanell, S. S. A., 2009, "Numerical Computations of Wind Turbine Wakes," Ph.D. thesis, Royal Institute of Technology, Stockholm, Sweden.
[9] Larsen, G. C., Madsen, H. Aa., Thomsen, K., and Larsen, T. J., 2008, "Wake Meandering—A Pragmatic Approach," Wind Energy, **11**, pp. 377–395.
[10] Vermeer, L. J., Sørensen, J. N., and Crespo, A., 2003, "Wind Turbine Aerodynamics," Prog. Aerosp. Sci., **39**, pp. 467–510.
[11] Ainslie, J. F., 1986, "Wake Modelling and the Prediction of Turbulence Properties," Proceedings of the Eighth British Wind energy Association Conference, Cambridge, Mar. 19–21, pp. 115–120.
[12] Ainslie, J. F., 1988, "Calculating the Flow Field in the Wake of Wind Turbines," J. Wind. Eng. Ind. Aerodyn., **27**, pp. 213–224.
[13] Madsen, H. A., Larsen, G. C., and Thomsen, K., 2005, "Wake Flow Characteristics in Low Ambient Turbulence Conditions," Proceedings of the Copenhagen Offshore Wind 2005.
[14] Madsen, H. Aa., Larsen, G. C., Larsen, T. J., Mikkelsen, R., and Troldborg, N., 2008, "Wake Deficit- and Turbulence Simulated With Two Models Compared With Inflow Measurements on a 2 MW Turbine in Wake Conditions," Scientific Proceedings of the 2008 European Wind Energy Conference and Exhibition, Brussels, Belgium, Mar. 31–Apr. 3, pp. 48–53.
[15] Ainslie, J. F., 1985, "Development of an Eddy Viscosity Model for Wind Turbine Wakes," Proceedings of the BWEA Conference, pp. 61–66.
[16] Panofsky, H. A., and Dutton, J. A., 1984, *Atmospheric Turbulence*, Wiley, New York.
[17] Mann, J., 1994, "The Spatial Structure of Neutral Atmospheric Surface-Layer Turbulence," J. Fluid Mech., **273**, pp. 141–168.
[18] Bingöl, F., Mann, J., and Larsen, G. C., 2010, "Lidar Measurements of Wake Dynamics. Part I: One Dimensional Scanning," Wind Energy, **13**, 51–61.
[19] Trujillo, J. J., Bingöl, F., Larsen, G. C., Mann, J., and Kühn, M., 2009, "Lidar Measurements of Wake Dynamics. Part II: Two Dimensional Scanning," Wind Energy, in press.
[20] Fluent, Inc., 1998, FIDAP 8 Theory Manual, Fluent Inc., Lebanon, NH.
[21] Madsen, H. Aa., 1996, "A CFD Analysis of the Actuator Disc Flow Compared With Momentum Theory Results," Proceedings of the IEA Joint Action of Tenth Symposium on Aerodynamics of Wind Turbines, B. M. Pedersen, ed., pp. 109–124.
[22] Madsen, H. Aa., 2000, "Yaw Simulation Using a 3*D* Actuator Disc Model Coupled to the Aeroelastic Code HawC," IEA Joint Action, Aerodynamics of Wind Turbines, 13th Symposium, B. M. Pedersen, ed., pp. 133–145.
[23] Madsen, H. Aa, Sørensen, N. N., and Schreck, S., 2003, "Yaw Aerodynamics Analyzed With Three Codes in Comparison With Experiment," 41st Aerospace Sciences Meeting and Exhibit, Reno, NV, Jan. 6–9, AIAA Paper No. 2003-519.
[24] Michelsen, J. A., 1994, "Basis 3*D*—A Plat-Form for Development of Multiblock PDE Solvers," Department of Fluid Mechanics, Technical University of Denmark, DTU, Report No. AFM 92-05,.
[25] Michelsen, J. A., 1994, "Block Structured Multigrid Solution of 2*D* and 3*D* Elliptic PDE's," Department of Fluid Mechanics, Technical University of Denmark, DTU, Report No. AFM 94-06.
[26] Sørensen, N. N., 1995, "General Purpose Flow Solver Applied to Flow over Hills," Ph.D. thesis, Risø National Laboratory, Technical University of Denmark, Roskilde, Denmark.
[27] Mikkelsen, R., Sørensen, J. N., and Troldborg, N., 2007, "Prescribed Wind Shear Modelling Combined With the Actuator Line Technique," Conference Proceedings of the EWEC 2007, Milano, Italy.
[28] Larsen, G. C., Madsen, H. Aa., Larsen, T. J., and Troldborg, N., 2008, "Wake Modeling and Simulation," Risø National Laboratory, Technical University of Denmark, Report No. Risø-R-1653(EN).
[29] Pope, S. B., 2000, "Turbulent Flows," Cambridge University Press, Cambridge, UK.
[30] Madsen, H. Aa., and Fischer, A., 2009, "Wind Shear and Turbulence Characteristics From Inflow Measurements on the Rotating Blade of a Wind Turbine Rotor," Scientific Proceedings of the 2009 European Wind Energy Conference and Exhibition, Marseille, France, Mar. 16–19, pp. 53–58.
[31] Jiminez, A., Crespo, A., Migoya, E., and Garcia, J., 2007, "Advances in Large Eddy Simulation of a Wind Turbine Wake," J. Phys.: Conf. Ser., **75**, p. 012041.
[32] Frandsen, S., and Thögersen, M. L., 1999, "Integrated Fatigue Loading for Wind Turbines in Wind Farms by Combining Ambient Turbulence and Wakes," Wind Eng., **23**(6), pp. 327–340.
[33] Quarton, D. C., and Ainslie, J. F., 1990, "Turbulence in Wind Turbine Wakes," Wind Eng., **14**(1), pp. 15–23.
[34] Crespo, A., and Hernandez, J., 1996, "Turbulence Characteristics in Wind-Turbine Wakes," J. Wind. Eng. Ind. Aerodyn., **61**, pp. 71–85.